Genomics Proteomics Bioinformatics 21 (2023) 742–755

Genomics Proteomics Bioinformatics

www.elsevier.com/locate/gpb
www.sciencedirect.com

ORIGINAL RESEARCH

m^{6}A Profile Dynamics Indicates Regulation of Oyster Development by m^{6}A-RNA Epitranscriptomes

Lorane Le Franc [1], Bruno Petton [2], Pascal Favrel [1], Guillaume Rivière [1,*]

[1] *Laboratoire de Biologie des Organismes et des Ecosystèmes Aquatiques (BOREA), Muséum d'Histoire Naturelle, Sorbonne Université, Université de Caen Normandie, Université des Antilles, CNRS UMR 8067, IRD, 14032 Caen, France*
[2] *Ifremer, Laboratoire des Sciences de l'Environnement Marin, UMR 6539 CNRS/UBO/IRD/Ifremer, Centre Bretagne, 29280 Plouzané, France*

Received 8 September 2021; revised 23 November 2022; accepted 2 December 2022
Available online 7 December 2022

Handled by Jianhua Yang

KEYWORDS

RNA methylation;
Transcription;
Embryo;
Metamorphosis;
Evo-devo

Abstract The N^6-methylation of RNA adenosines (N^6-methyladenosine, m^{6}A) is an important regulator of gene expression with critical implications in vertebrate and insect development. However, the developmental significance of epitranscriptomes in lophotrochozoan organisms remains unknown. Using methylated RNA immunoprecipitation sequencing (MeRIP-seq), we generated transcriptome-wide m^{6}A-RNA methylomes covering the entire development of the oyster from oocytes to juveniles. Oyster RNA classes display specific m^{6}A signatures, with messenger RNAs (mRNAs) and long non-coding RNAs (lncRNAs) exhibiting distinct profiles and being highly methylated compared to transposable element (TE) transcripts. Epitranscriptomes are dynamic and correspond to the chronological steps of development (cleavage, gastrulation, organogenesis, and **metamorphosis**), with minimal mRNA and lncRNA methylation at the morula stage followed by a global increase. mRNA m^{6}A levels are correlated with transcript levels, and shifts in methylation profiles correspond to expression kinetics. Differentially methylated transcripts cluster according to **embryo**-larval stages and bear the corresponding developmental functions (cell division, signal transduction, morphogenesis, and cell differentiation). The m^{6}A level of TE transcripts is also regulated and peaks during the gastrulation. We demonstrate that m^{6}A-RNA methylomes are dynamic and associated with gene expression regulation during oyster development. The putative epitranscriptome implication in the cleavage, maternal-to-zygotic transition, and cell differentiation in a lophotrochozoan model brings new insights into the control and evolution of developmental processes.

* Corresponding author.
E-mail: guillaume.riviere@unicaen.fr (Rivière G).

Peer review under responsibility of Beijing Institute of Genomics, Chinese Academy of Sciences / China National Center for Bioinformation and Genetics Society of China.

https://doi.org/10.1016/j.gpb.2022.12.002

Introduction

The success of development of metazoan organisms is conditioned by the precise temporo-spatial regulation of gene expression. The N^6-methylation of RNA adenosines (N^6-methyladenosine, m^6A) has recently emerged as a critical layer of the gene expression regulatory network. Indeed, m^6A-RNA methylation is required in vertebrates for the proper regulation of developmental processes such as cell differentiation [1,2], X chromosome inactivation [3,4], maternal-to-zygotic transition (MZT) [5,6], and neurogenesis [7–9]. Besides, the invalidation of enzymes which deposit m^6A on RNA is lethal during the early development [10,11].

The m^6A-RNA is regulated by an enzymatic machinery comprising writers and erasers. The METTL3/METTL14/WTAP writer core complex [12] deposits methyl marks at the consensus sequence DRACH (D = A/G/T, R = A/G, H = A/C/T) [13–16]. Erasers like ALKBH5 [17] and the controversial FTO [18] remove methylation. The combined action of m^6A writers and erasers makes m^6A profiles highly dynamic during the development of investigated species [6,19,20].The biological effects of RNA methylation are mediated by reader proteins able to bind m^6A. For example, the YTH protein family of readers is involved in RNA stability, translation level [21–24], splicing [25], and nuclear export [26]. Other readers like hnRNPA2B1 [27], IGF2BP [28], and Prrc2a [8] mediate m^6A influence on RNA stability, and eIF3a guides cap-independent translation of m^6A-RNAs [29]. This whole machinery allows to guide the methylation on specific RNA targets and modulates their cellular fate. As a result, m^6A is a chemical modification that influences gene expression without modifying the nucleic acid sequence of associated transcript and is therefore referred to as "epitranscriptomic" [30].

Many RNA classes are subjected to m^6A methylation, which is the most abundant internal modification in eukaryotic messenger RNAs (mRNAs). m^6A modifications in mRNAs are mostly found in the 3′ untranslated regions (3′ UTRs) at the vicinity of the stop codon [13,14,31]. However, m^6A is also present at lower levels in 5′ UTRs [29,32], long internal exons [15,31], and introns [16,33].

Although m^6A modification is well described in mRNA targets, it also affects most non-coding RNAs (ncRNAs) including microRNAs (miRNAs) [27], circular RNAs (circRNAs) [34], small nuclear RNAs (snRNAs) [35], and small nucleolar RNAs (snoRNAs) [36]. In vertebrates, more than 300 long non-coding RNAs (lncRNAs) are m^6A-methylated [14]. Such modification alters the RNA structure toward an increased protein accessibility [37], as well as subcellular localization [38]. The m^6A of lncRNAs has critical developmental outcomes, as indicated by the requirement of m^6A of the *Xist* lncRNA for the transcriptional silencing of the inactivated X chromosome [4]. Besides, the m^6A in RNAs encoded by transposable element (TE) genes (*i.e.*, repeat RNAs) increases their stability and promotes chromatin compaction [39].

Aside from vertebrates, the m^6A has been described in a wide diversity of organisms, such as insects [40–42], yeasts [43], and plants [44]. However, despite the developmental significance of m^6A being conserved across the evolution, several differences exist between animal groups. Indeed, in fruit flies, m^6A is mostly present in the 5′ UTRs of mRNAs throughout head and embryo development [42,45], whereas m^6A enrichment at 5′ UTRs promotes cap-independent translation for transcript selection during the stress response in vertebrates [29,32,46]. In the silkworm (*Bombyx mori*), mRNAs are mostly methylated in coding sequences (CDSs) but not in UTRs, and a high methylation level is associated with a high gene expression level [47]. Besides, a higher m^6A content and gene expression regulation is found upstream the diapause [41], a development phase which is reflective of a highly plastic phenotype. Finally, in *Caenorhabditis elegans*, in which only few actors of the m^6A machinery are present, methylation is mostly found in ribosomal RNAs (rRNAs) [48]. This situation opens crucial questions about the evolution of m^6A-related molecular pathways, target genes, and developmental significance that require investigations in divergent models. However, despite being of upmost importance for our understanding of the evolution of the molecular control of developmental processes, there is a critical lack of knowledge in lophotrochozoan organisms in which epitranscriptomes were not investigated to date to our knowledge.

The Pacific oyster *Crassostrea gigas* (*i.e.*, *Magallana gigas*) is a bivalve mollusk whose great ecological and economical significance allow it to emerge as a model species within lophotrochozoan organisms. As such, an important amount of genetic, transcriptomic, and epigenetic data have been generated in this model [49–51]. Besides, the embryo-larval development of *C. gigas* is under the strong epigenetic influence of DNA methylation [52–54] and histone marks [55,56]. Moreover, it has recently been demonstrated that m^6A and its complete associated machinery are conserved in oysters, with features strongly indicating an epitranscriptomic regulation of development [57]. Furthermore, oysters develop as pelagic larvae in sea water before they metamorphose into fixed adult specimen. Therefore, the early-life stages of oysters are directly subjected to the variations of external environmental conditions such as temperature changes, ultraviolet (UV) exposure, or endocrine disruptor contamination, which are described to influence m^6A-RNA in investigated species [29,46,58–60]. These elements are highly suggestive of a functional significance of m^6A-RNA in oyster development, which remains unknown to date.

To investigate these questions, we characterized the transcriptome-wide dynamics of m^6A-RNA methylomes across the entire development of the Pacific oyster from the oocytes to the completion of the organogenesis. We used methylated RNA immunoprecipitation sequencing (MeRIP-seq) to investigate and monitor the dynamics of m^6A levels, localization, target RNA subsets, and functional implications in a lophotrochozoan model to provide a better understanding of the evolution of developmental mechanisms and their epigenetic regulation.

Results

Oyster RNA classes display specific m^6A signatures

In developing oysters, m^6A methylation affects a vast majority of RNA classes, and is detected in 91.0% of mRNAs, 65.7% of lncRNAs, 87.0% of RNA TEs (*i.e.*, retrotransposons), and 99.4% of DNA TEs. In contrast, oyster transfer RNAs (tRNAs) are mostly unmethylated (rRNAs were depleted

during library preparation and not investigated here). In addition, 35.8% of mRNAs and 11.1% of lncRNAs are significantly m^{6}A-enriched over background levels (Figure 1A). The methylation pattern depends on the RNA class considered [Kolmogorov–Smirnov (KS) test, $P < 7.55 \times 10^{-11}$]. Although m^{6}A in mRNAs is found from the 5′ UTR to the 3′ UTR, and is more abundant around the stop codon, it is more randomly spread along lncRNAs (Figure 1B). Methylation affects adenosines located within the "AGUGA*C" sequence (where * marks the modified adenosine) (Figure 1C). The mean methylation level differs between RNA classes, and DNA TE transcripts are less methylated than mRNAs, lncRNAs, and RNA TEs (Figure 1D). The MeRIP-seq procedure was validated by investigation of the status of five transcripts exhibiting contrasted m^{6}A *vs.* mRNA profiles in other species (*c-myc*, *klf*, *mettl3*, *hnrnpa2b1*, and *oct4*) by targeted methylated RNA immunoprecipitation followed by quantitative polymerase chain reaction (MeRIP-qPCR) [15,28,32,61]. All the examined candidates displayed similar patterns between the two techniques, and those patterns are consistent with the literature (Figure S1).

Oyster m^{6}A epitranscriptomes are dynamic and correspond to defined steps of the development chronology

The principal component analysis (PCA) of MeRIP-seq data indicates that the samples group together according to the embryo-larval stages and are overall organized chronologically along the X-axis (PC1) (Figure 2A). The PCA plot can be divided into four areas defining four developmental phases: cleavage (from oocytes to 2-to-8-cell stage), gastrulation (blastula and gastrula stages), tissue differentiation (trochophore and D-larvae stages), and metamorphosis (pediveliger and spat stages). The morula stage is clearly individualized along the PC2, suggesting peculiar m^{6}A methylation and development features. This segregation is confirmed by the pairwise correlation matrix (Figure 2B). The chronological segregation of developmental stages according to m^{6}A methylation indicates that m^{6}A-RNA epitranscriptomes are an important component of the developmental process.

The m^{6}A epitranscriptomes are dynamic during oyster development. There is an important decrease in the number of methylated transcripts at the morula stage followed by a

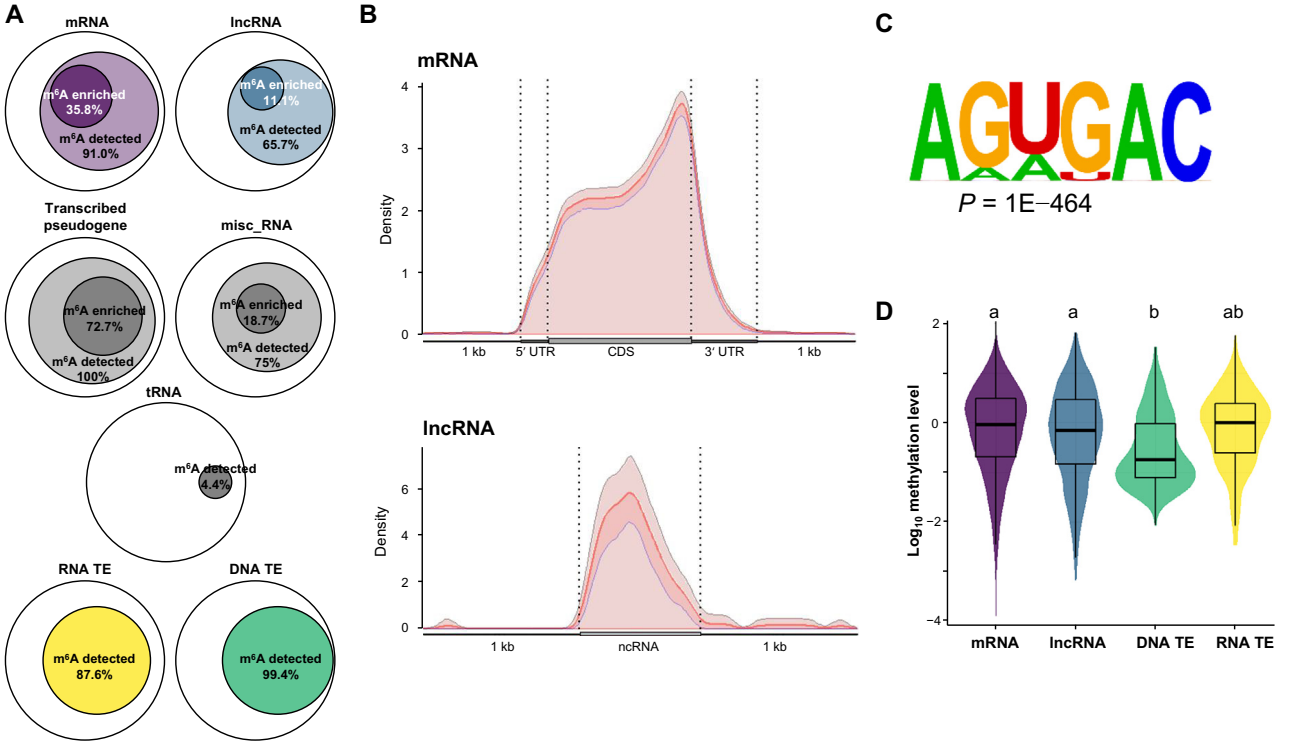

Figure 1 m^{6}A signatures of oyster RNA classes

A. m^{6}A distribution among RNA classes. Diagram diameter was normalized between RNA classes. The internal circles in diagrams represent the proportion of RNA displaying significant m^{6}A methylation over background (light color) and significant m^{6}A enrichment (dark color), respectively. **B.** m^{6}A localization along mRNAs and lncRNAs (5′ to 3′). The mean m^{6}A density and confidence interval are represented. **C.** Consensus sequence of the m^{6}A motif in the oyster identified by HOMER. **D.** Mean methylation level of the methylated transcripts of mRNA, lncRNA, DNA TE, and RNA TE classes during oyster development. Letters discriminate significantly different methylation levels (ANOVA followed by Bonferroni's post hoc test, $P < 0.05$). mRNA, messenger RNA; lncRNA, long non-coding RNA; DNA TE, DNA transposable element; RNA TE, retrotransposon; misc_RNA, miscellaneous RNA; tRNA, transfer RNA; ncRNA, non-coding RNA; ANOVA, analysis of variance; UTR, untranslated region; CDS, coding sequence; kb, kilobase.

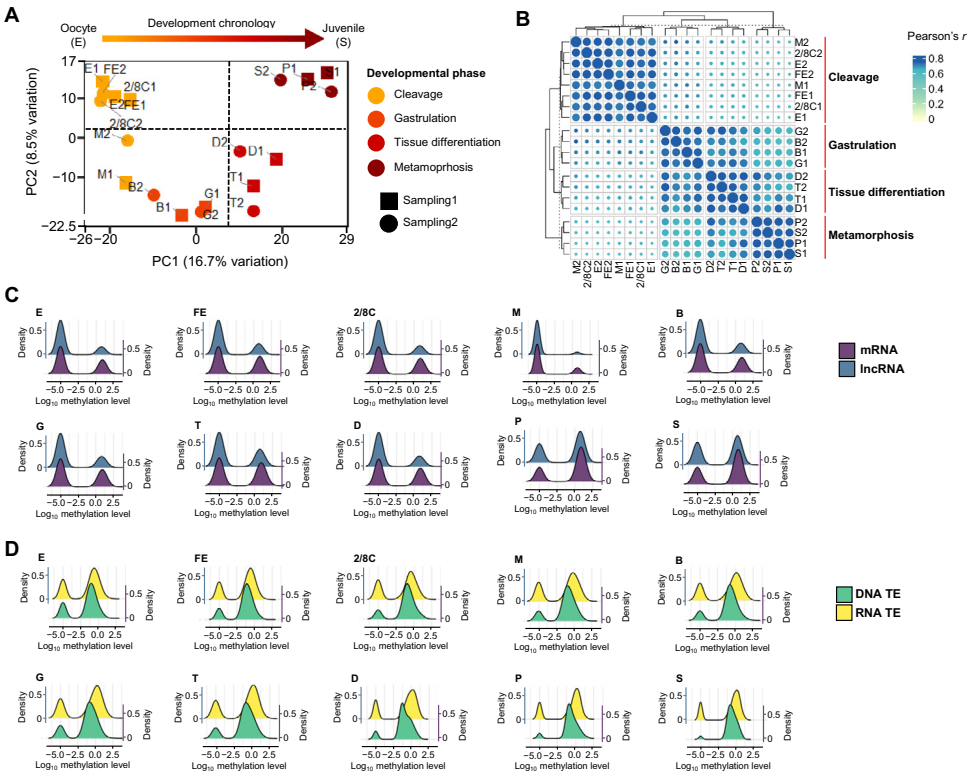

Figure 2 Epitranscriptome dynamics during oyster development

A. PCA of MeRIP-seq results. **B.** Similarity (pairwise Pearson's correlation matrix) of m^{6}A methylation between samples based on IP/Input signal (see Materials and methods). IP indicates the immunoprecipitated fraction, and Input indicates the input fraction. **C.** Dynamics of the m^{6}A methylation level of the mRNA (purple) and lncRNA (blue) transcripts. All the transcripts found m^{6}A-enriched over background using MetPeak in at least one development stage are represented. Areas under the curve are normalized for each RNA class, and undetectable methylation at certain stages was arbitrarily affected a value of −5 for representation purpose. **D.** Dynamics of the m^{6}A methylation level of the DNA TE (green) and RNA TE (yellow) transcripts. All the transcripts found m^{6}A-enriched over background using MetPeak in at least one development stage are represented. Areas under the curve are normalized for each RNA class, and undetectable methylation at certain stages was arbitrarily affected a value of −5 for representation purpose. E, egg (oocyte); FE, fertilized egg; 2/8C, 2-to-8-cell stage; M, morula; B, blastula; G, gastrula; T, trochophore; D, D-larva; P, pediveliger; S, spat/juvenile; PCA, principal component analysis; MeRIP-seq, methylated RNA immunoprecipitation sequencing; PC, principal component.

general shift toward increased m^{6}A mRNAs and lncRNAs onward, which is particularly noticeable at the late development stages (*i.e.*, pediveliger and spat stages) (Figure 2C). The same tendency is also observed, although to a lesser extent, for RNA TE, whose unmethylated population becomes reduced in the late developmental phases (Figure 2D).

mRNA m^{6}A profiles are regulated and correlated to gene expression levels and kinetics throughout oyster development

The mRNA m^{6}A methylation is highly dynamic during oyster development. Indeed, among the significantly methylated mRNAs [analysis of variance (ANOVA), $P < 0.05$; $n = 8404$], 17.8% of m^{6}A-mRNAs ($n = 1494$) display a significant variation in their m^{6}A levels (**Figure 3**A), and these m^{6}A levels are significantly correlated to their expression levels (Figure 3B). The differentially methylated m^{6}A-mRNAs define four clusters according to their methylation (and expression) profiles, corresponding to the developmental steps defined previously. Cluster 1 includes mRNAs with a strong methylation and transcript content in the early stages (up to the morula stage) which decreases afterward. By contrast, the mRNAs within the three other clusters display poor methylation during the early stages, which strongly increases from the gastrulation (Cluster 2), the trochophore stage (Cluster 3), and the pediveliger stage (Cluster 4), and remain strongly methylated afterward. Overall, there is a marked decrease of m^{6}A methylation at the morula stage.

Besides the level of methylation, the localization of m^{6}A within mRNAs can also vary between clusters (KS test, $0.31 < P < 5.11 \times 10^{-12}$ depending on cluster pairwise comparison). Indeed, Cluster 1 mRNAs, which are essentially maternal mRNAs, are methylated mostly around their stop codon in oocytes and thereafter. By contrast, mRNAs within the three other clusters, that are essentially expressed from the zygotic genome, display a marked biphasic profile, with an increased 5′ m^{6}A content at the vicinity of the CDS start (Figure 3C). However, this pattern shifts toward a less biphasic profile with m^{6}A becoming relatively more dominant around the stop codon in the later development stages when the methylation and expression levels increase (KS test, $5.87 \times 10^{-7} < P < 5.35 \times 10^{-10}$ depending on the cluster).

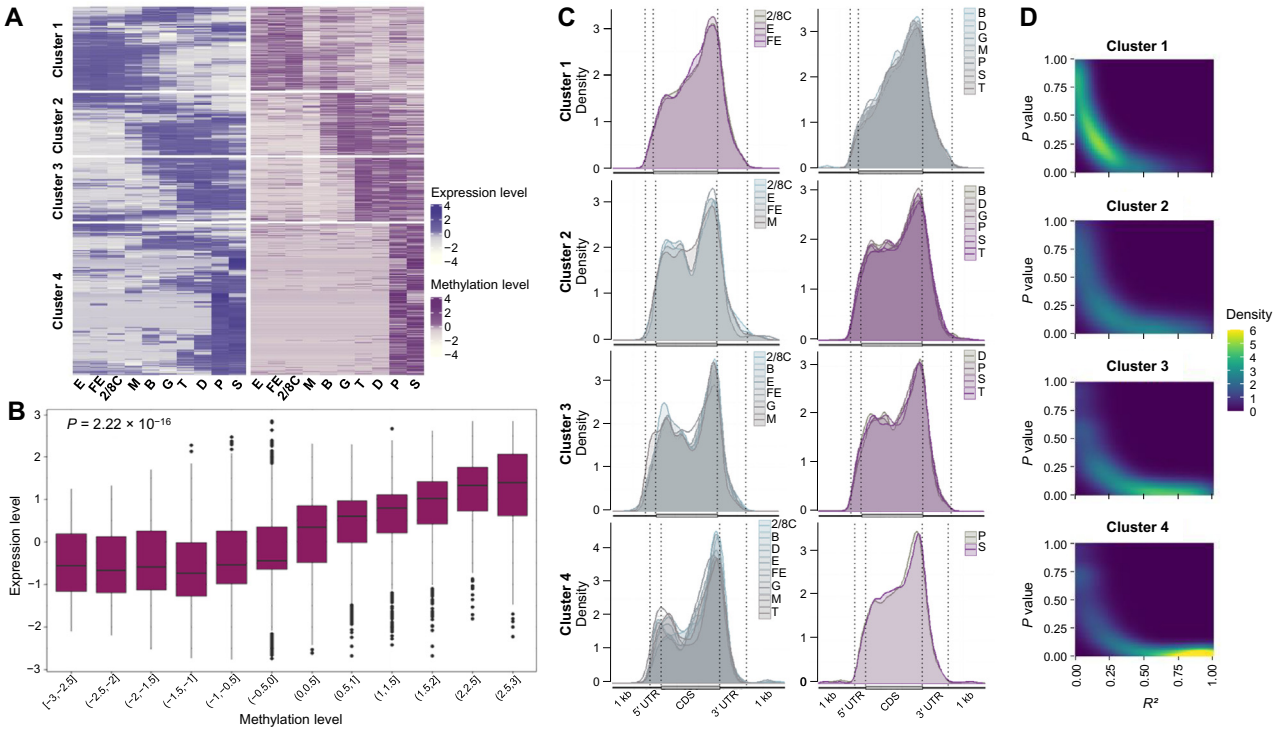

Figure 3 Dynamics of mRNA expression and m^{6}A methylation during oyster development

A. Normalized expression (TPM, purple) and m^{6}A content (IP/Input, pink) of significantly differentially methylated mRNA genes during oyster development (n = 1494). The development stages are indicated below. **B.** Correlation between expression (Y-axis, TPM) and methylation (X-axis, IP/Input, divided into twelve quantiles). **C.** Methylation profiles of mRNAs displaying high (pink) or low (gray) expression within each cluster. The development stages in high and low expression groups are indicated (mean m^{6}A density; confidence intervals were omitted for clarity). **D.** Correlation of expression *vs.* methylation dynamics throughout development. The linear correlation of the methylation variation *vs.* expression variation was assessed for each gene across oyster development per cluster and the results are given as surface plots (R^2, X-axis; P value, Y-axis; density of genes, Z-axis). Yellow color in the right bottom corner (*i.e.*, $P < 0.05$ and $R^2 > 0.5$) indicates strong correlation. TPM, transcripts per million.

Furthermore, these m^{6}A-mRNAs have their methylation and expression dynamics strongly correlated (Clusters 2, 3, and 4), whereas early differentially methylated transcripts without 5′ CDS methylation do not (Cluster 1) (Figure 3D). This indicates that mRNA expression dynamics are correlated with m^{6}A profile dynamics after, but not before, the zygotic genome activation. Together, these results bring to light a regulation of gene expression by both the level and localization of m^{6}A methylation across oyster developmental stages.

Differentially m^{6}A methylated mRNAs bear the corresponding developmental functions

Gene Ontology (GO) analysis of differentially methylated m^{6}A-mRNAs shows an overall term enrichment related to developmental processes, like morphogenesis and mesoderm development (**Figure 4**; Table S1). More specific functions correspond to each methylation cluster. Cluster 1 (cleavage) is enriched in terms related to the cell division whereas later clusters (gastrulation, tissue differentiation, and metamorphosis) bear terms that may be more a reflection of signal transduction associated with cell differentiation such as the TGFβ/SMAD pathway. These results point to a functional implication of the m^{6}A in the regulation of oyster developmental processes.

ncRNA transcript content is also associated with m^{6}A profiles

Similar to mRNAs, lncRNAs can be grouped into clusters according to the developmental chronology of their m^{6}A dynamics, with the highest methylation levels during the early stages for a cleavage cluster (Cluster 1), during the gastrulation and tissue type differentiation (Cluster 2), and at the pediveliger and spat stages for a metamorphosis cluster (Cluster 3), respectively. A marked decrease in m^{6}A levels at the morula stage is also observed for lncRNAs (**Figure 5**A). The methylation and expression levels are positively correlated overall (Figure 5B), although the methylation and expression dynamics are correlated only for the "late" Clusters 2 and 3, but not for the "early" Cluster 1 (Figure 5C).

m^{6}A methylation in RNA TEs and DNA TEs is regulated across oyster development

The methylation of RNA TEs is mostly represented by the methylation of long terminal repeat (LTR) and long interspersed nuclear element (LINE) groups (62.93% and 31.46%, respectively). With 85.5% and 100% of transcripts being methylated, respectively. Their methylation levels display a peak at the blastula and trochophore stages for LTR

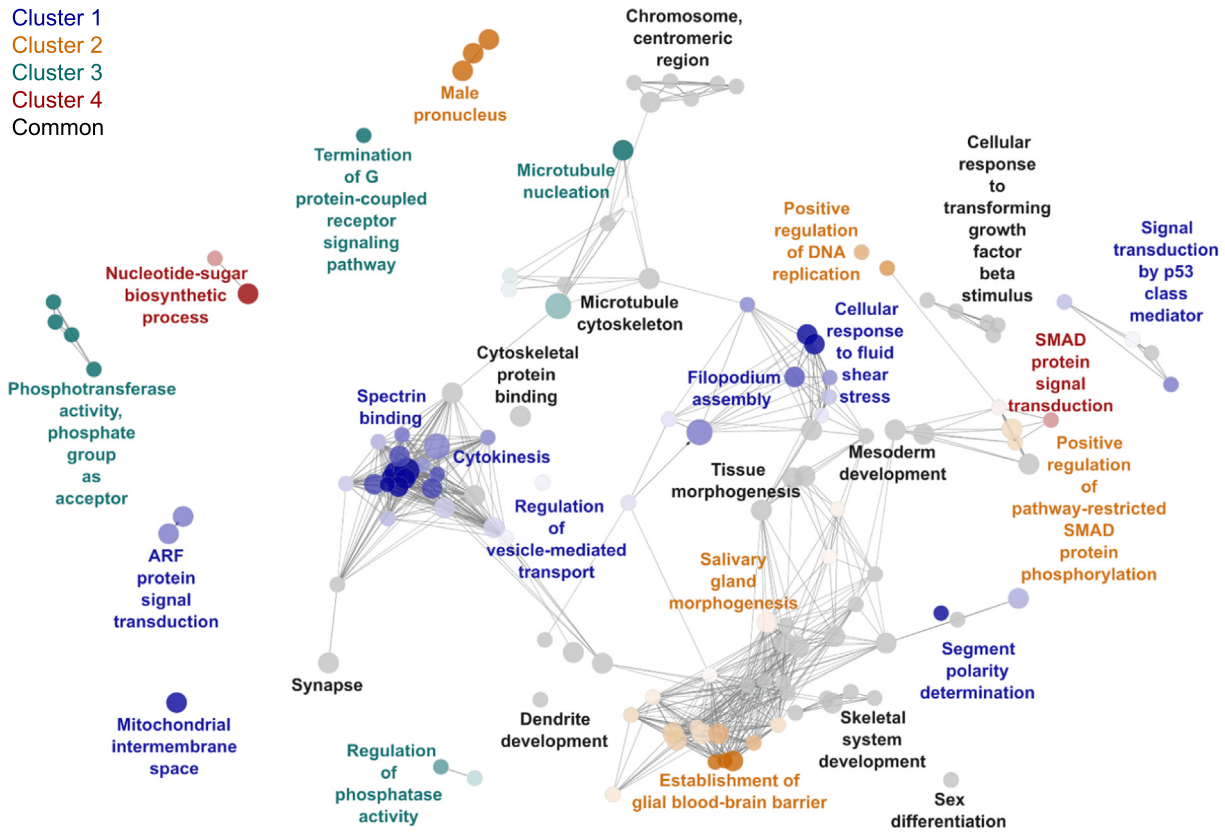

Figure 4 Functional annotation of differentially methylated mRNAs during oyster development
Enriched GO terms (hypergeometric test, FDR < 0.05) associated with differential m^{6}A mRNA methylation across oyster development. Enriched terms corresponding to specific clusters are colored, and common terms between clusters are in black. Color intensity is relative to cluster specificity, with color limit set to 51% of genes inside the respective clusters. Circle diameter is inversely proportional to the *P* value of the enrichment. GO, Gene Ontology; FDR, false discovery rate.

and LINE, respectively (Figure 6A). Both the DNA TE and RNA TE (retrotransposon) methylation levels were dynamic during oyster development (ANOVA, $P < 0.05$). Terminal inverted repeat (TIR; 37.13%), Helitron (32.50%), and Crypton (20.25%) are the three main DNA TE types whose transcripts are the most methylated and represented 92.6%, 88.5%, and 100% of transcripts in each type, respectively. Their m^{6}A levels are the highest around the gastrulation, and Helitron TEs exhibit an additional peak in pediveliger larvae (Figure 6B). These results show that the m^{6}A methylation of TE transcripts displays class-specific dynamics during oyster development that are different from mRNAs and lncRNAs.

Discussion

This work presents the profiling of m^{6}A epitranscriptomes during the development of the oyster *C. gigas* from the egg to the completion of organogenesis. We demonstrate that the methylation of RNA is dynamic throughout the oyster's early life and specific to the RNA population considered. The methylation kinetics of mRNAs defines clusters corresponding to the chronology of development, which is correlated with gene expression level and dynamics, and the genes whose transcripts display m^{6}A regulation bear developmental functions. lncRNAs display similar profiles whereas TE transcripts have a specific signature with a peak in m^{6}A levels during gastrulation. Our study provides evidence for a developmental significance of m^{6}A epitranscriptomes at various levels in oysters.

The distinct oyster RNA classes present specific m^{6}A signatures and vary in terms of methylation level and location. Indeed, although mRNAs are m^{6}A-modified from the CDS start but mostly around the stop codon, lncRNAs do not present a biased methylation enrichment at their 3′ end. This result, suspected from our previous measurements of global m^{6}A content in polyA *vs.* total RNA [57], is more consistent with what is observed in human embryonic cell types [16] than in insects in which methylated adenosines are mostly lying in the 5′ UTR and CDS [19,42,47]. This finding is rather surprising because insects are ecdysozoans which are considered the "sister clade" of lophotrochozoans within protostomes. Nevertheless, this assumption is increasingly moderated by the closer resemblance of molecular features in mollusks and annelids to vertebrates, *i.e.*, deuterostomes, rather than to ecdysozoan features [54,62,63]. Overall, m^{6}A are found in oysters within the motif "DRA*C" which contains the GAC consensus sequence which is widely conserved across the evolution [14,19,40,43,44]. The repetitive nature of TE sequences only allows a less precise analysis of their m^{6}A features compared with other RNA classes. However, we find that oysters' DNA TE transcripts

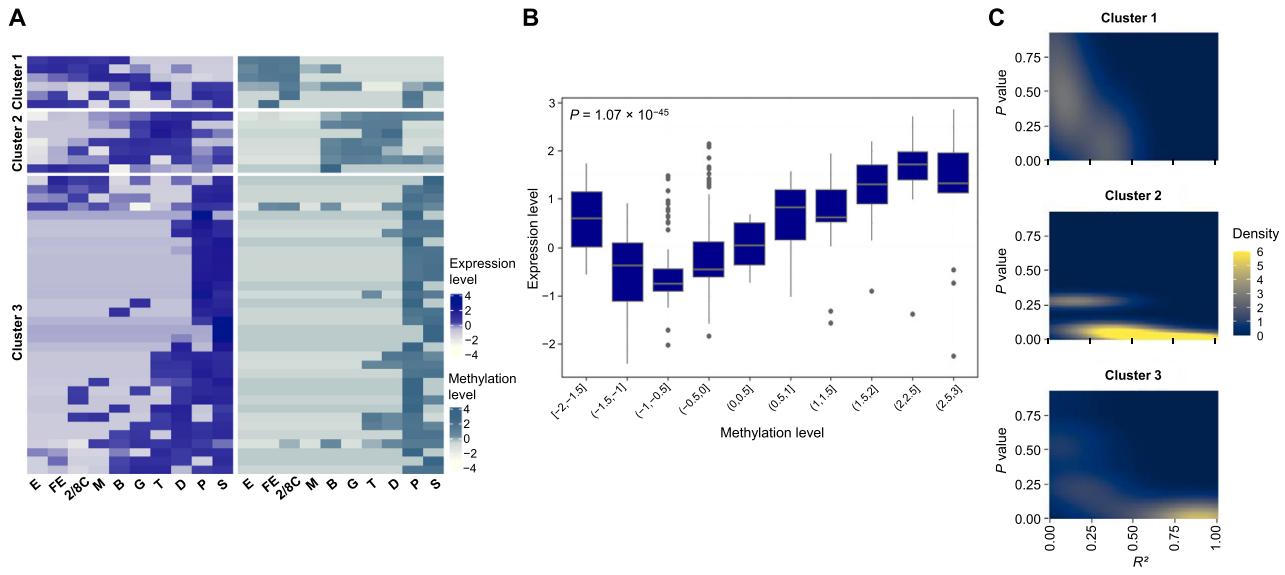

Figure 5 Dynamics of lncRNA expression and m^{6}A methylation during oyster development

A. Normalized expression (blue) and m^{6}A content (turquoise) of significantly methylated lncRNA genes during oyster development. Transcript variants were pooled for each gene. **B.** Correlation between expression (Y-axis) and methylation (X-axis) levels. The methylation level was divided into ten quantiles. **C.** Correlation plot of expression *vs.* methylation dynamics throughout development. The linear correlation of the methylation *vs.* expression variation was assessed for each gene across oyster development per cluster, and the results are given as surface plots (R^2, X-axis; *P* value, Y-axis; density of genes, Z-axis).

are significantly less methylated than RNA TEs, which is in line with observations made in *Arabidopsis* [64].

Oyster epitranscriptomes are dynamic and associated with defined successive developmental steps, namely cleavage, gastrulation, tissue differentiation, and metamorphosis. The similarity of m^{6}A profiles in eggs before and after fertilization suggests a poor contribution of sperm to embryonic m^{6}A methylomes, which is consistent with the sperm scarce RNA content regarding the oocyte stock. Epitranscriptomes clearly shift during the developmental chronology, with a marked decrease of m^{6}A levels in mRNA and lncRNA transcripts at the end of cleavage followed by a gradual increase, and a maximum methylation reached at the pre-metamorphosis stage that remains high afterward in juveniles. The morula stage constitutes a pivot point in which the methylation of mRNAs and lncRNAs, but not of RNA TEs, is strongly depleted. Interestingly, based on transcriptomic [65] and 5mC-DNA methylation data [52], this stage could be considered an important window of MZT in the oyster, when most maternal RNA resources are consumed and early transcriptional events occur [66]. Interestingly, the marked epitranscriptomic features at cleavage and metamorphosis may remind of the important shifts in 5mC-DNA profiles (decrease during cleavage and important levels prior to metamorphosis) [52] and could suggest an interplay between the epigenetic layers in the regulation of oyster development, possibly through competition for methyl donor [67] or histone-related pathways [68,69]. This observation is reminiscent of the crosstalk between the 5mC-DNA status of the Pou5f1 pioneer stem cell factor promoter and the m^{6}A methylation of its transcript in humans [16], hence raising the question of m^{6}A-modified transcripts in the oyster development.

The m^{6}A content and transcript abundance of differentially methylated mRNAs are positively correlated across oyster development, which surprisingly contrasts with the case of the honeybee in which highly methylated transcripts exhibit down-regulated expression [19], thus further indicating an evolutionary divergence between mollusks and insects regarding epitranscriptomic mechanisms. Overall, oyster differentially methylated mRNAs have functions related to developmental processes, which further confirms the developmental significance of the epitranscriptomic regulation in the oyster. More precisely, differentially methylated mRNA transcripts group into four clusters that match the development steps described above, whose GO annotations assess the functional relevance in the cognate developmental processes (Cluster 1, cleavage; Cluster 2, gastrulation; Cluster 3, tissue differentiation; and Cluster 4, metamorphosis). However, these clusters do not always display similar methylation profiles neither correlations between m^{6}A and expression level dynamics.

Cluster 1 mRNA transcripts are highly methylated and abundant during the cleavage. They are present in oocytes and therefore correspond to maternal transcripts. Although their expression and methylation levels are dramatically reduced at the onset of MZT (morula stage), their m^{6}A and transcript content dynamics are not significantly correlated, and they display predominant methylation around the stop codon throughout oyster development. Such m^{6}A profiles promote mRNA degradation via interaction with readers such as YTHDF proteins during cleavage in other species [5,70], and we showed that an oyster YTHDF orthologue is present at high levels in this window [57]. Besides, Cluster 1 differentially methylated mRNAs bear functions in the cytoskeleton processes of cytokinesis. Together, these results indicate that the

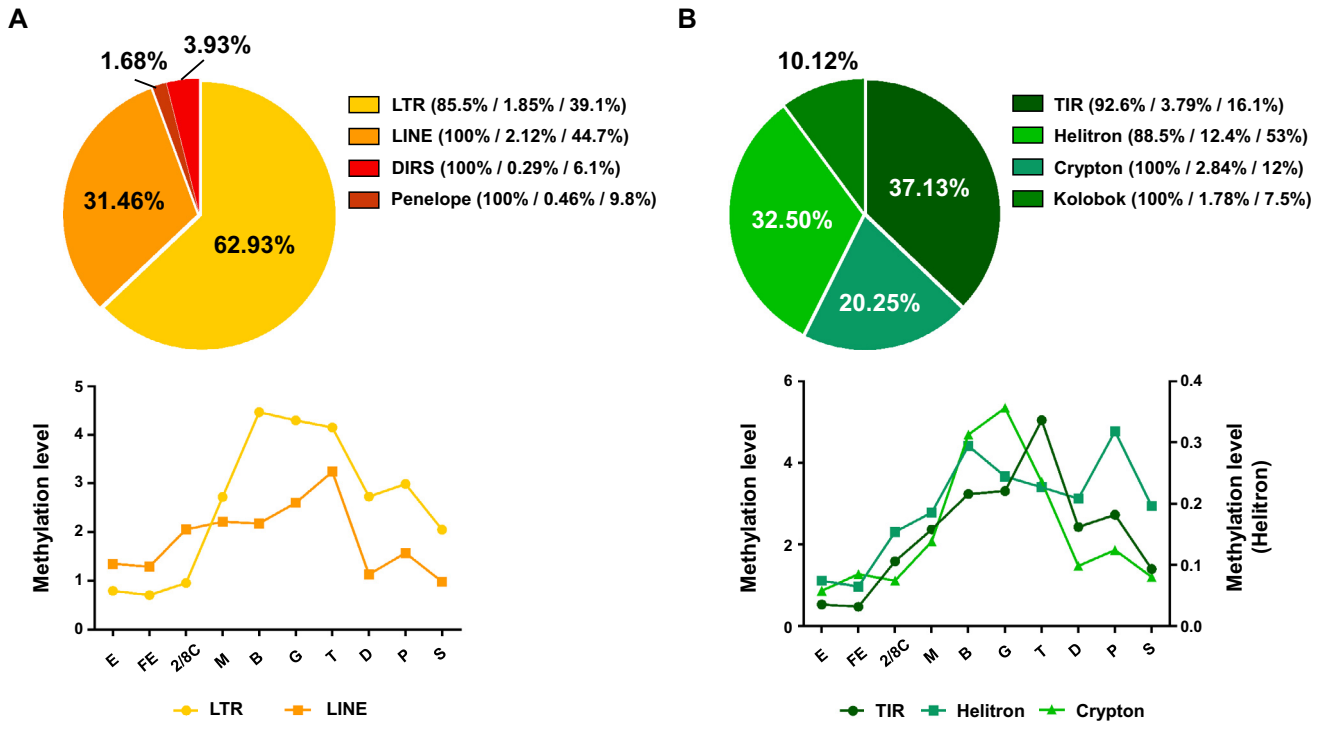

Figure 6 m^{6}A dynamics of TE transcripts during oyster development

A. m^{6}A dynamics of RNA TE transcripts during oyster development. Top: relative representation of methylated RNA TE transcripts. The percentages in parenthesis indicate the proportion of transcripts methylated in the TE class, the initial proportion of the TE class in the genome, and the proportion of the TEs investigated, respectively. Bottom: relative representation of methylation level variation during oyster development. **B.** m^{6}A dynamics of DNA TE transcripts during oyster development. Top: relative representation of methylated DNA TE transcripts. The percentages in parenthesis indicate the proportion of transcripts methylated in the TE class, the initial proportion of the TE class in the genome, and the proportion of the TEs investigated, respectively. Bottom: relative representation of methylation level variation during oyster development. Values are given as the mean of the two independent experiments. Only TEs representing more than 20% of their class are represented. Error bars were omitted for clarity. Reference methylation level is the mean methylation level of RNA TE or DNA TE in oocytes. LTR, long terminal repeat; LINE, long interspersed nuclear elements; TIR, terminal inverted repeat; DIRS, *Dictyostelium* intermediate repeat sequence.

oyster MZT may be triggered by YTHDF-mediated decay of maternal mRNAs, whose translation is important for cell proliferation during cleavage. We hypothesize that the depletion of the cytokinesis machinery mRNA templates of maternal origin below a certain threshold, and/or the putative associated slowdown of cell divisions, may participate in triggering the zygotic genome activation. It remains to be deciphered whether and how such signals could be interpreted in terms of cell fate decisions.

Clusters 2, 3, and 4, respectively, correspond to the gastrulation, the setting up of differentiated tissues, and the metamorphosis. In contrast to Cluster 1, their m^{6}A pattern is dynamic and shifts from bimodal profiles in early stages to a late mostly unimodal m^{6}A distribution around the stop codon. Such 5′-enriched m^{6}A profiles are observed in plants [44], *Xenopus* [71], mice [2], and fruit flies [45], and may be associated with increased RNA turnover and fast transcript processing depending on the positioning of methylation in the CDS or 5′ UTR. Consistently, in developing oysters, the early bimodal m^{6}A distribution is associated with a low transcript abundance. The 3′ patterns are associated with the recruitment of readers such as YTHDC1 [25,72,73], IGF2BP [28], or Prrc2a [8], and mediate translation initiation during gastrulation, as well as splicing and RNA trafficking during cell type differentiation. In oysters, the later sequential shift of clusters toward more 3′-dominant methylation is correlated with an increased expression level of the differentially methylated mRNA transcripts. Furthermore, those transcripts that become successively methylated and expressed bear the cognate developmental functions such as mesoderm specification, morphogenesis, and signal transduction related to cell differentiation. In addition, readers including YTHDCs, IGF2BP, and Prrc2a are functional in oysters and present in stage-specific sets after the MZT [57], and METTL3 expression is also dramatically increased after the MZT and sustained later on. Together, this strongly suggests that m^{6}A regulates gene expression toward cell differentiation upon the zygotic genome activation, possibly by promoting translation via transcript selection and increased mRNA stability. As suggested by GO annotation, m^{6}A likely participates in mesoderm formation during gastrulation via a METTL3-dependent regulation of epithelial to mesenchymal transition, as described in human cancer cells [74,75]. Our findings (Table S1) are also consistent with the METTL3/YTHDF2-dependent osteoblast differentiation by SMAD inhibitor downregulation in mammalian cells [76,77]. Regarding the conservation of the TGFβ pathway in

oyster development [78,79], these results may also suggest feedback loops between TGFβ signaling and m^{6}A regulation in the control of (pluri)potency during differentiation [80].

lncRNA methylation levels display similar developmental dynamics to mRNAs, although m^{6}A modifications are not preferentially located at their 3′-end. Like mRNAs, the methylation levels in lncRNAs are also correlated with their transcript content and dynamics after the MZT. How lncRNA epitranscriptomes might participate in oyster development is less clear because oyster lncRNAs are poorly conserved and annotated. Besides, their limited number compared with mRNAs in addition to the limited resolution of MeRIP-seq did not allow the detection of m^{6}A peak localization shifts. Nevertheless, the vertebrate writer complex cofactor RBM15/15B and the hnRNPA2B1 nuclear complex are conserved in oysters [57]. Therefore, we speculate that oyster lncRNA epitranscriptomes could regulate the chromatin state and transcription in an m^{6}A-dependent manner, which is somewhat reminiscent of the *Xist*-mediated silencing [3,4], MALAT1-mediated stimulation [81], and/or chromosome-associated regulatory RNA (carRNA) switches in mammals [39]. However, *Xist* is not conserved in oysters and further work is required to test this hypothesis.

TE transcripts display class-specific dynamics during oyster development that are different from mRNAs and lncRNAs. Both RNA TEs and DNA TEs, which are poorly m^{6}A modified during cleavage, exhibit higher methylation during gastrulation and cell differentiation. Although the role of epitrancriptomes in TE control remains largely unknown, this kinetics may suggest the participation of m^{6}A within the widely conserved RNA mechanisms of TE silencing required for cell differentiation [82–84].

Altogether, our results demonstrate that oyster m^{6}A epitranscriptomes are dynamic and RNA-class specific, and reveal their implication in oyster MZT and sequential expression of genes required for gastrulation, cell differentiation, and metamorphosis. Although additional studies would be required to determine the interplay of m^{6}A-RNA with the epigenetic network and the underlying mechanisms, this first evidence of an epitranscriptomic regulation of development in a lophotrochozoan species allows for a better understanding of developmental processes and their evolution.

Materials and methods

Animals

Broodstock oysters, embryos, larvae, and spat were obtained at the Ifremer marine facility (Argenton, France) as previously described [52,85]. Briefly, gametes of mature broodstock oysters were obtained by stripping the gonads and filtering the recovered material on a 60-μm mesh to remove large debris. Oocytes were collected as the remaining fraction on a 20-μm mesh and spermatozoa as the passing fraction on a 20-μm mesh. Oocytes were pre-incubated in 5 l of UV-treated and 1-μm mesh filtered sterile sea water (SSW) at 21 °C until germinal vesicle breakdown. Fertilization was triggered by the addition of *ca.*10 spermatozoids per oocyte. After the expulsion of the second polar body was assessed by light microscopy, embryos were transferred in 150-l tanks of oxygenated SSW at 21 °C. The embryonic stages were determined by light microscopy observation. The embryonic stages collected were oocytes (E, immediately before sperm addition), fertilized oocytes (FE, immediately before transfer to 150-l tanks), 2-to-8-cell embryos [2/8C, *ca.* 1.5 h post fertilization (hpf)], morula (M, *ca.* 4 hpf), blastula (B, *ca.* 6 hpf), gastrula (G, *ca.* 10 hpf), trochophore (T, *ca.* 16 hpf), and D larvae (D, *ca.* 24 hpf). For pediveliger (P) and spat (S) stages, D-larvae were collected and reared in a flow-through rearing system at 21.5 °C in SSW. At the end of the pelagic stage, competent larvae were collected on a 100-μm mesh to allow the larval settlement. At 20 days post fertilization (dpf) the pediveliger stage was sampled as the remaining fraction on a 400-μm mesh. The post-larvae were maintained in a downwelling system. Then, at 25 dpf the spat stage was sampled after metamorphosis as the remaining fraction on a 400-μm mesh.

For each embryonic stage, 3 million embryos were collected as the remaining fraction on a 20-μm mesh and centrifuged at 123 *g* for 5 min at room temperature. The supernatant was discarded and samples of 1 million embryos were then snap-frozen in liquid nitrogen directly after resuspension in TRI Reagent (Catalog No. T9424, Sigma-Aldrich, St Louis, MO; 1 ml/1 × 10^6 embryos). For pediveliger and spat samples, 100 mg of each stage were resuspended in TRI Reagent (Catalog No. T9424, Sigma-Aldrich; 1 ml/100 mg) and snap-frozen in liquid nitrogen. All samples were stored at −80 °C. Two distinct experiments were realized (February and March 2019) using the gametes of 126 and 140 broodstock animals, respectively (Figure S2).

RNA extraction and fragmentation

RNA of each development stage was extracted using phenol–chloroform followed by affinity chromatography as previously described [86]. Briefly, embryos were ground in TRI Reagent (Catalog No. T9424, Sigma-Aldrich), and RNA was purified using affinity chromatography with NucleoSpin RNA Clean Up Kit (Catalog No. 740948, Macherey-Nagel, Duren, Germany). Potential contaminating DNA was removed by digestion with rDNase (Catalog No. 740963, Macherey-Nagel) according to the manufacturer's instructions for 15 min at 37 °C, and then RNA was purified using Agencourt AMPure XP solid-phase reversible immobilization (SPRI) paramagnetic beads (Catalog No. A63880, Beckman Coulter, Brea, CA) according to the manufacturer's instructions. Briefly, paramagnetic beads and RNA were mixed slowly and incubated for 5 min at room temperature followed by 2 min on a magnetic rack. The cleared supernatant was removed, and beads were washed three times with 70% ethanol. After 4 min of drying at room temperature, RNA was mixed slowly with RNase free water and incubated for 1 min at room temperature on the magnetic rack. The eluted total RNA was stored at −80 °C.

The RNA was heat-fragmented as previously described [87]. Briefly, for each RNA sample (development stages and pools of development stages), 5 μg of total RNA was suspended in 18 μl of RNase free water. The RNA was fragmented by the addition of 2 μl of fragmentation buffer [100 mM Tris-HCl pH 7.0, 100 mM $ZnCl_2$, diethylpyrocarbonate-treated (DEPC) water] and incubated for 2 min at 70 °C. After the incubation, 2 μl of ethylenediaminetetraacetic acid (EDTA) 0.5 M was immediately added, and

RNA was incubated on ice for 2 min to stop the reaction. Then, RNA was purified using Agencourt AMPure XP SPRI paramagnetic beads (Catalog No. A63880, Beckman Coulter) as previously described and eluted in 50 µl of RNase free water. The fragment size (*ca.* 100 nt) was verified by fluorescent capillary electrophoresis using an Agilent 2100 Bioanalyzer with Agilent RNA 6000 Pico Kit (Catalog No. 5067-1513, Agilent, Santa Clara, CA) according to the manufacturer's instruction.

MeRIP

The MeRIP-seq of total RNA was performed on fragmented RNA. Of the 50 µl fragmented RNA solution, 5 µl (*i.e.*, corresponding to 500 ng of starting RNA before fragmentation) was non immunoprecipitated and used as the input fraction (Input), and 44 µl (*i.e.*, corresponding to 4.5 µg of starting RNA before fragmentation) were subjected to m^{6}A-immunoprecipitation using m^{6}A antibody-coupled Pierce Protein A/G Magnetic Beads (Catalog No. 88803, ThermoFisher Scientific, Waltham, MA) following the low/high salt procedure by Zeng and collaborators [87]. For each sample, 30 µl of protein A and 30 µl of protein G magnetic beads were incubated on a magnetic rack and washed twice with immunoprecipitation (IP) buffer (150 mM NaCl, 10 mM Tris-HCl pH 7.5, IGEPAL 0.1%, DEPC water) and resuspended in 500 µl of IP buffer. The magnetic beads were incubated overnight at 4 °C under gentle shaking with 5 µg of anti-m^{6}A antibody (Catalog No. ABE572, Millipore, Burlington, MA). Then magnetic beads were washed twice with IP buffer and resuspended in RNA mixture composed of 100 µl of 5× IP buffer, 44 µl of fragmented RNAs, and 200 units of RNasin Plus Ribonuclease Inhibitor (Catalog No. N2611, Promega, Madison, WI), and the mixture was completed to 500 µl with IP buffer. The obtained MeRIP solution containing magnetics beads coupled to antibody and RNA fragments was incubated for 2 h at 4 °C with gentle shaking. After incubation, the MeRIP solution was incubated on a magnetic rack and the supernatant was removed. Beads were washed twice in IP buffer, twice in low salt buffer (50 mM NaCl, 10 mM Tris-HCl pH 7.5, 0.1% IGEPAL, DEPC water), and twice in high salt buffer (500 mM NaCl, 10 mM Tris-HCl pH 7.5, 0.1% IGEPAL, DEPC water) for 10 min at 4 °C with gentle shaking for each washing step. After extensive washing with IP buffer, RNA fragments hybridized to the antibody-coated magnetic beads were resuspended in 200 µl of RA1 buffer supplied in the NucleoSpin RNA Clean Up Kit (Catalog No. 740948, Macherey Nagel, Duren, France) and incubated for 2 min at room temperature then 1 min on a magnetic rack. The supernatant containing immunoprecipitated RNA was collected and mixed with 400 µl of 100% ethanol. Then the immunoprecpitated RNA was purified using affinity chromatography with NucleoSpin RNA Clean Up Kit (Catalog No. 740948, Macherey Nagel) and eluted twice with 14 µl of RNase free water. These immunoprecipitated RNA fragments correspond to the immunoprecipitated fraction (IP).

Reverse transcription-quantitative polymerase chain reaction

To validate the IP of m^{6}A methylated RNA, a reverse transcription-quantitative polymerase chain reaction (RT-qPCR) was performed on immunoprecipitated RNA pools. These pools are composed of equal amounts of RNA from each developmental stage for the two distinct experiments. Input and IP fractions were obtained as described above. The equivalent amount of 1.75 ng of Input and IP RNA were used as starting template for the RT-qPCR protocol previously described [86]. Targets included one reference transcript (*ef1α*) and five conserved genes exhibiting distinct transcript m^{6}A methylation in vertebrates (*c-myc*, *klf*, *mettl3*, *hnrnpa2b1*, and *oct4*). Briefly, RNA was reverse-transcribed using 200 U of M-MLV Reverse Transcriptase (Catalog No. M1701, Promega) and 100 ng random hexamers. Resulting cDNA was assayed for target gene expression using the Input expression as a reference. SYBR Green quantitative PCR was performed on a CFX96 apparatus (Catalog No. 1845096, Bio-Rad, Marnes-la-Coquette, France). Gotaq qPCR Master Mix (Catalog No. A6002, Promega) was used in 40 cycles (95 °C/15 s and 60 °C/15 s) reactions. Target genes included one reference gene and five target genes with distinct transcript m^{6}A methylation in vertebrates, and were amplified with the following primers: *Cg-ef1α* (CGI_10012474, LOC105338957; forward: 5′-ACCACCCTGGTGAGATCAAG-3′, reverse: 5′-ACGACGATCGCATTTCTCTT-3′) as reference transcript of gene expression in *C. gigas* [51], genes described as methylated in vertebrates: *Cg-c-myc* (CGI_10002799, LOC105341025; forward: 5′-CGGTCTCTCCCAAATTCTCCC-3′, reverse: 5′-TGCTACTTCCACTTGCCCTG-3′) [15,28], *Cg-klf* (CGI_10019173, LOC105329817; forward: 5′-GAAATCTCCGATGTTGCTGG-3′, reverse: 5′-CTTTCCACGGTATTTGCGAG-3′) [15], *Cg-mettl3* (CGI_10023713, LOC105329074; forward: 5′-TGGAACCAAAGAAGAGTGTCAGA-3′, reverse: 5′-AGAAATGAACAGTCTCCAAGGGA-3′) [32], and *Cg-hnrnpa2b1* (CGI_10028469, LOC105333434; forward: 5′-CCAGGGAGGCTACAATGAAGG-3′, reverse: 5′-ACACCACCACCAAAGCTGTT-3′) [61], and a gene described as not methylated in vertebrates: *Cg-oct4* (XM_034479449, LOC117680409; forward: 5′-GTGAAAGGTGCGCTAGAAAA-3′, reverse: 5′-GGACCACTTCTTTCTCCAGT-3′) [15]. The methylation level was calculated as the normalized ratio of the IP signals and the Input signals by the formula $2^{-\Delta(Ct\ IP-Ct\ Input)}$. The gene expression level was assayed on the Input fractions, normalized on the reference transcript *ef1α* [51], and given by the formula $2^{-\Delta Ct}$.

Library preparation and sequencing

Amounts equivalent to 1.125 µg of starting RNA of the IP fraction (*i.e.*, 3.5 µl of the eluted IP fraction) and to the 50 ng of starting RNA of the Input fraction for each sample, respectively, were used for library construction using the SMARTer Stranded Total RNA-Seq Kit v.2 (Catalog No. 634418, Pico Input Mammalian, Takara/Clontech, Saint-Germain-en-Laye, France) according to the manufacturer's protocol without RNA fragmentation. The ribosomal cDNA depletion step and a final cDNA amplification of 16 cycles were performed. Paired-end 150-bp sequencing of Input and IP cDNA libraries of each sample were conducted on an Illumina HiSeq 4000 platform (Catalog No. SY-401-4001, Illumina, San Diego, CA) at the Genome Quebec Innovation Center (McGill University, Montréal, Canada).

MeRIP-seq data analyses

Read quality was evaluated using FastQC (v.0.11.7) and MultiQC (v.1.7), and adaptor sequences and low-quality reads were removed using Trimmommatic (v.0.38). The remaining reads were aligned to the oyster genome v.9 (GCF_000297895.1), and uniquely mapped reads were counted using STAR (v.2.7.3a) with the parameter "-quantMode GeneCounts" [88]. mRNA and ncRNA were identified from the gene annotation, and TEs were identified using the RepeatMasker annotation output provided with assembly data. The expression level in all Input samples was expressed in transcripts per million (TPM) [89]. The identification of m^{6}A-enriched peaks was performed on uniquely mapped reads of the IP samples using SAMtools (v.1.9) and MeTPeak R package [90] [false discovery rate (FDR) < 5%] with the cognate Input samples as controls. The methylation level of these m^{6}A-enriched RNAs corresponds to the mean of the IP/Input fold change provided by MeTPeak from the two development experiments. The distribution of m^{6}A across mRNAs and ncRNAs was visualized using Guitar plots [91]. The methylation level of TEs was assessed as the ratio of IP/Input with reads per gene expressed in TPM. Transcript variants were pooled for each gene, and only the transcripts that were present in the two distinct development experiments were considered expressed or methylated in Input and IP data, respectively. The gene expression and m^{6}A level are expressed as the mean of the two replicates of development stages from the independent experiments.

The m^{6}A motif was searched in the 1000 m^{6}A peaks presenting the lowest FDR and the highest IP/Input fold change using HOMER (v.4.10.4). The motif length was restricted to 5–6 nt. All peaks mapped on mRNAs and ncRNAs were used as the target sequences, and the background sequences were constituted of 5% of the Input reads (pool of February development experiment sample) selected randomly using SAMtools (v.1.9).

GO analysis

The RNA sequences identified as differentially methylated across oyster development were identified using BLASTN [92–94] against the GigaTON reference transcriptome database [65] with default settings. GO analyses were carried out with the GO annotations obtained from the GigaTON database gene universe [65]. GO term enrichment tests were performed using ClueGO plugin (v.2.5.7) [95] on Cytoscape (v.3.8.0). The hypergeometric test with a FDR < 5% was used to consider significant GO term enrichment.

Statistical analyses and graph production

The m^{6}A level variation across oyster development was analyzed using one-way ANOVA (factor: development stage) followed by Bonferroni's post hoc test when required, unless otherwise stated. m^{6}A level variations were computed on significantly methylated mRNAs and lncRNAs (*e.g.*, "enriched" RNA according to MeTPeak results) and on RNA TEs displaying detectable methylation because of limitations in their accurate location within the genome due to their repetitive sequences. The values were log-centered and reduced for heatmap production when stated. Methylation profiles were compared using KS tests (CDS regions were divided into 20 bins, whereas start and stop codon intervals as well as 5′ UTRs and 3′ UTRs were left unmodified from the default MetPeak output). The correlation between methylation level and transcript content across oyster development, as well as methylation variation and transcript content variation between stages, was estimated using linear regression. $P < 0.05$ was considered significant. All bioinformatic analyses (unless otherwise stated) were performed using R (v.3.6.3) and RStudio (v.1.0.153) software. The R packages *eulerr* [96], *ComplexHeatmap* [97], *ggplot2* [98], *Guitar* [91], PCAtools (2022; https://bioconductor.org/packages/release/bioc/vignettes/PCAtools/inst/doc/PCAtools.html), and Prism v.6 (GraphPad) software were used for figure production. All authors have read and approved the final manuscript.

Data availability

All data relative to this study have been deposited in the National Center for Biotechnology Information Gene Expression Omnibus (GEO: GSE18038), and are publicly accessible at https://www.ncbi.nlm.nih.gov/geo/, and have also been deposited in the Genome Sequence Archive [99] at the National Genomics Data Center, Beijing Institute of Genomics, Chinese Academy of Sciences / China National Center for Bioinformation (GSA: CRA007976), and are publicly accessible at https://ngdc.cncb.ac.cn/gsa.

Competing interests

The authors have declared no competing interests.

CRediT authorship contribution statement

Lorane Le Franc: Methodology, Software, Validation, Formal analysis, Investigation, Data curation, Writing – original draft, Writing – review & editing, Visualization. **Bruno Petton:** Investigation, Resources, Writing – review & editing. **Pascal Favrel:** Writing – review & editing, Funding acquisition. **Guillaume Rivière:** Conceptualization, Methodology, Software, Validation, Formal analysis, Investigation, Resources, Writing – original draft, Writing – review & editing, Visualization, Supervision, Project administration, Funding acquisition. All authors have read and approved the final manuscript.

Acknowledgments

This work was supported by the French national program CNRS EC2CO ECODYN (Ecosphère Continentale et Côtière 'HERITAGe'; Grant No. 2019-200919362L) awarded to Guillaume Rivière and the Council of the Normandy Region (RIN ECUME; Grant No. 18E01643-18P02383) awarded to Pascal Favrel.

Supplementary material

Supplementary data to this article can be found online at https://doi.org/10.1016/j.gpb.2022.12.002.

ORCID

ORCID 0000-0002-4051-4415 (Lorane Le Franc)
ORCID 0000-0002-4169-2811 (Bruno Petton)
ORCID 0000-0002-2504-9957 (Pascal Favrel)
ORCID 0000-0001-8372-8715 (Guillaume Rivière)

References

[1] Zhang M, Zhai Y, Zhang S, Dai X, Li Z. Roles of N^6-methyladenosine (m^6A) in stem cell fate decisions and early embryonic development in mammals. Front Cell Dev Biol 2020;8:782.
[2] Chang M, Lv H, Zhang W, Ma C, He X, Zhao S, et al. Region-specific RNA m^6A methylation represents a new layer of control in the gene regulatory network in the mouse brain. Open Biol 2017;7:170166.
[3] Coker H, Wei G, Moindrot B, Mohammed S, Nesterova T, Brockdorff N. The role of the *Xist* 5′ m^6A region and RBM15 in X chromosome inactivation. Wellcome Open Res 2020;5:31.
[4] Patil DP, Chen CK, Pickering BF, Chow A, Jackson C, Guttman M, et al. m^6A RNA methylation promotes *XIST*-mediated transcriptional repression. Nature 2016;537:369–73.
[5] Zhao BS, Wang X, Alana V, Lu Z, Shi H, Kuuspalu A, et al. m^6A-dependent maternal mRNA clearance facilitates zebrafish maternal-to-zygotic transition. Nature 2017;542:475–8.
[6] Sui X, Hu Y, Ren C, Cao Q, Zhou S, Cao Y, et al. METTL3-mediated m^6A is required for murine oocyte maturation and maternal-to-zygotic transition. Cell Cycle 2020;19:391–404.
[7] Yoon KJ, Ringeling FR, Vissers C, Jacob F, Pokrass M, Jimenez-Cyrus D, et al. Temporal control of mammalian cortical neurogenesis by m^6A methylation. Cell 2017;171:877–89.
[8] Wu R, Li A, Sun B, Sun JG, Zhang J, Zhang T, et al. A novel m^6A reader Prrc2a controls oligodendroglial specification and myelination. Cell Res 2019;29:23–41.
[9] Edens BM, Vissers C, Su J, Arumugam S, Xu Z, Shi H, et al. FMRP modulates neural differentiation through m^6A-dependent mRNA nuclear export. Cell Rep 2019;28:845–54.
[10] Geula S, Moschitch-Moshkovitz S, Dominissini D, Mansour AA, Kol N, Salmon-Divon M, et al. m^6A mRNA methylation facilitates resolution of naïve pluripotency toward differentiation. Science 2015;347:1002–6.
[11] Wang Y, Li Y, Toth JI, Petroski MD, Zhang Z, Zhao JC. N^6-methyladenosine modification destabilizes developmental regulators in embryonic stem cells. Nat Cell Biol 2014;16:191–8.
[12] Yang Y, Hsu PJ, Chen Y, Yang YS. Dynamic transcriptomic m^6A decoration: writers, erasers, readers and functions in RNA metabolism. Cell Res 2018;28:616–24.
[13] Ke S, Alemu EA, Mertens C, Gantman EC, Fak JJ, Mele A, et al. A majority of m^6A residues are in the last exons, allowing the potential for 3′ UTR regulation. Genes Dev 2015;29:2037–53.
[14] Meyer KD, Saletore Y, Zumbo P, Elemento O, Mason CE, Jaffrey SR. Comprehensive analysis of mRNA methylation reveals enrichment in 3′ UTRs and near stop codons. Cell 2012;149:1635–46.
[15] Batista PJ, Molinie B, Wang J, Qu K, Zhang J, Li L, et al. m^6A RNA modification controls cell fate transition in mammalian embryonic stem cells. Cell Stem Cell 2014;15:707–19.
[16] Xiao S, Cao S, Huang Q, Xia L, Deng M, Yang M, et al. The RNA N^6-methyladenosine modification landscape of human fetal tissues. Nat Cell Biol 2019;21:651–61.
[17] Zheng G, Dahl JA, Niu Y, Fedorcsak P, Huang CM, Li CJ, et al. ALKBH5 is a mammalian RNA demethylase that impacts RNA metabolism and mouse fertility. Mol Cell 2013;49:18–29.
[18] Jia G, Fu Y, Zhao X, Dai Q, Zheng G, Yang Y, et al. N^6-methyladenosine in nuclear RNA is a major substrate of the obesity-associated FTO. Nat Chem Biol 2011;7:885–7.
[19] Wang M, Xiao Y, Li Y, Wang X, Qi S, Wang Y, et al. RNA m^6A modification functions in larval development and caste differentiation in honeybee (*Apis mellifera*). Cell Rep 2021;34:108580.
[20] Zhang Y, Xiang Y, Yin Q, Du Z, Peng X, Wang Q, et al. Dynamic epigenomic landscapes during early lineage specification in mouse embryos. Nat Genet 2018;50:96–105.
[21] Wang X, Zhao BS, Roundtree IA, Lu Z, Han D, Ma H, et al. N^6-methyladenosine modulates messenger RNA translation efficiency. Cell 2015;161:1388–99.
[22] Wang X, Lu Z, Gomez A, Hon GC, Yue Y, Han D, et al. N^6-methyladenosine-dependent regulation of messenger RNA stability. Nature 2014;505:117–20.
[23] Hsu PJ, Zhu Y, Ma H, Guo Y, Shi X, Liu Y, et al. Ythdc2 is an N^6-methyladenosine binding protein that regulates mammalian spermatogenesis. Cell Res 2017;27:1115–27.
[24] Shi H, Wang X, Lu Z, Zhao BS, Ma H, Hsu PJ, et al. YTHDF3 facilitates translation and decay of N^6-methyladenosine-modified RNA. Cell Res 2017;27:315–28.
[25] Xiao W, Adhikari S, Dahal U, Chen YS, Hao YJ, Sun BF, et al. Nuclear m^6A reader YTHDC1 regulates mRNA splicing. Mol Cell 2016;61:507–19.
[26] Roundtree IA, Luo GZ, Zhang Z, Wang X, Zhou T, Cui Y, et al. YTHDC1 mediates nuclear export of N^6-methyladenosine methylated mRNAs. Elife 2017;6:e31311.
[27] Alarcón CR, Goodarzi H, Lee H, Liu X, Tavazoie S, Tavazoie SF. HNRNPA2B1 is a mediator of m^6A-dependent nuclear RNA processing events. Cell 2015;162:1299–308.
[28] Huang H, Weng H, Sun W, Qin X, Shi H, Wu H, et al. Recognition of RNA N^6-methyladenosine by IGF2BP proteins enhances mRNA stability and translation. Nat Cell Biol 2018;20:285–95.
[29] Meyer KD, Patil DP, Zhou J, Zinoviev A, Skabkin MA, Elemento O, et al. 5′ UTR m^6A promotes cap-independent translation. Cell 2015;163:999–1010.
[30] Saletore Y, Meyer K, Korlach J, Vilfan ID, Jaffrey S, Mason CE. The birth of the epitranscriptome: deciphering the function of RNA modifications. Genome Biol 2012;13:175.
[31] Dominissini D, Moshitch-moshkovitz S, Schwartz S, Salmon-Divon M, Ungar L, Osenberg S, et al. Topology of the human and mouse m^6A RNA methylomes revealed by m^6A-seq. Nature 2012;485:201–6.
[32] Coots RA, Liu XM, Mao Y, Dong L, Zhou J, Wan J, et al. m^6A facilitates eIF4F-independent mRNA translation. Mol Cell 2017;68:504–14.
[33] Louloupi A, Ntini E, Conrad T, Ørom UAV. Transient N^6-methyladensosine transcriptome sequencing reveals a regulatory role of m^6A in splicing efficiency. Cell Rep 2018;23:3429–37.
[34] Yang Y, Fan X, Mao M, Song X, Wu P, Zhang Y, et al. Extensive translation of circular RNAs driven by N^6-methyladenosine. Cell Res 2017;27:626–41.
[35] Warda AS, Kretschmer J, Hackert P, Lenz C, Urlaub H, Höbartner C, et al. Human METTL16 is a N^6-methyladenosine (m^6A) methyltransferase that targets pre-mRNAs and various non-coding RNAs. EMBO Rep 2017;18:2004–14.
[36] Huang L, Ashraf S, Wang J, Lilley DM. Control of box C/D snoRNP assembly by N^6-methylation of adenine. EMBO Rep 2017;18:1631–45.
[37] Liu N, Zhou KI, Parisien M, Dai Q, Diatchenko L, Pan T. N^6-methyladenosine alters RNA structure to regulate binding of a low-complexity protein. Nucleic Acids Res 2017;45:6051–63.
[38] Wu Y, Yang X, Chen Z, Tian L, Jiang G, Chen F, et al. m^6A-induced lncRNA RP11 triggers the dissemination of colorectal cancer cells via upregulation of Zeb1. Mol Cancer 2019;18:87.

[39] Liu J, Dou X, Chen C, Chen C, Liu C, Xu MM, et al. N^6-methyladenosine of chromosome-associated regulatory RNA regulates chromatin state and transcription. Science 2020;367:580–6.
[40] Lence T, Akhtar J, Bayer M, Schmid K, Spindler L, Ho CH, et al. m^{6}A modulates neuronal functions and sex determination in *Drosophila*. Nature 2016;540:242–7.
[41] Jiang T, Li J, Qian P, Xue P, Xu J, Chen Y, et al. The role of N^6-methyladenosine modification on diapause in silkworm (*Bombyx mori*) strains that exhibit different voltinism. Mol Reprod Dev 2019;86:1981–92.
[42] Kan L, Grozhik AV, Vedanayagam J, Patil DP, Pang N, Lim KS, et al. The m^{6}A pathway facilitates sex determination in *Drosophila*. Nat Commun 2017;8:15737.
[43] Bodi Z, Button JD, Grierson D, Fray RG. Yeast targets for mRNA methylation. Nucleic Acids Res 2010;38:5327–35.
[44] Luo GZ, Macqueen A, Zheng G, Duan H, Dore LC, Lu Z, et al. Unique features of the m^{6}A methylome in *Arabidopsis thaliana*. Nat Commun 2014;5:5630.
[45] Worpenberg L, Paolantoni C, Longhi S, Mulorz MM, Lence T, Wessels HH, et al. Ythdf is a N^6-methyladenosine reader that modulates Fmr1 target mRNA selection and restricts axonal growth in *Drosophila*. EMBO J 2021;40:e104975.
[46] Zhou J, Wan J, Gao X, Zhang X, Jaffrey SR, Qian SB. Dynamic m^{6}A mRNA methylation directs translational control of heat shock response. Nature 2015;526:591–4.
[47] Li B, Wang X, Li Z, Lu C, Zhang Q, Chang L, et al. Transcriptome-wide analysis of N^6-methyladenosine uncovers its regulatory role for gene expression in lepidopteran *Bombyx mori*. Insect Mol Biol 2019;28:703–15.
[48] Sendinc E, Valle-Garcia D, Jiao A, Shi Y. Analysis of m^{6}A RNA methylation in *Caenorhabditis elegans*. Cell Discov 2020;6:47.
[49] Zhang G, Fang X, Guo X, Li L, Luo R, Xu F, et al. The oyster genome reveals stress adaptation and complexity of shell formation. Nature 2012;490:49–54.
[50] Riviere G, Wu GC, Fellous A, Goux D, Sourdaine P, Favrel P. DNA methylation is crucial for the early development in the oyster *C. gigas*. Mar Biotechnol 2013;15:739–53.
[51] Dheilly NM, Lelong C, Huvet A, Favrel P. Development of a Pacific oyster (*Crassostrea gigas*) 31,918-feature microarray: identification of reference genes and tissue-enriched expression patterns. BMC Genomics 2011;12:468.
[52] Riviere G, He Y, Tecchio S, Crowell E, Gras M, Sourdaine P, et al. Dynamics of DNA methylomes underlie oyster development. PLoS Genet 2017;13:e1006807.
[53] Sussarellu R, Lebreton M, Rouxel J, Akcha F, Rivière G. Copper induces expression and methylation changes of early development genes in *Crassostrea gigas* embryos. Aquat Toxicol 2018;196:70–8.
[54] Saint-Carlier E, Riviere G. Regulation of *Hox* orthologues in the oyster *Crassostrea gigas* evidences a functional role for promoter DNA methylation in an invertebrate. FEBS Lett 2015;589:1459–66.
[55] Fellous A, Favrel P, Guo X, Riviere G. The Jumonji gene family in *Crassostrea gigas* suggests evolutionary conservation of Jmj-C histone demethylases orthologues in the oyster gametogenesis and development. Gene 2014;538:164–75.
[56] Fellous A, Lefranc L, Jouaux A, Goux D, Favrel P, Rivière G. Histone methylation participates in gene expression control during the early development of the Pacific oyster *Crassostrea gigas*. Genes 2019;10:695.
[57] Le Franc L, Bernay B, Petton B, Since M, Favrel P, Rivière G. A functional m^{6}A-RNA methylation pathway in the oyster *Crassostrea gigas* assumes epitranscriptomic regulation of lophotrochozoan development. FEBS J 2021;288:1696–711.
[58] Lu Z, Ma Y, Li Q, Liu E, Jin M, Zhang L, et al. The role of N^6-methyladenosine RNA methylation in the heat stress response of sheep (*Ovis aries*). Cell Stress Chaperones 2019;24:333–42.
[59] Xiang Y, Laurent B, Hsu CH, Nachtergaele S, Lu Z, Sheng W, et al. m^{6}A RNA methylation regulates the UV-induced DNA damage response. Nature 2017;543:573–6.
[60] Cayir A, Barrow TM, Guo L, Byun HM. Exposure to environmental toxicants reduces global N^6-methyladenosine RNA methylation and alters expression of RNA methylation modulator genes. Environ Res 2019;175:228–34.
[61] Kwon J, Jo YJ, Namgoong S, Kim NH. Functional roles of hnRNPA2/B1 regulated by METTL3 in mammalian embryonic development. Sci Rep 2019;9:8640.
[62] Cho SJ, Valles Y, Giani Jr VC, Seaver EC, Weisblat DA. Evolutionary dynamics of the *wnt* gene family: a lophotrochozoan perspective. Mol Biol Evol 2010;27:1645–58.
[63] Nederbragt AJ, van Loon AE, Dictus WJAG. Hedgehog crosses the snail's midline. Nature 2002;417:811–2.
[64] Wan Y, Tang K, Zhang D, Xie S, Zhu X, Wang Z, et al. Transcriptome-wide high-throughput deep m^{6}A-seq reveals unique differential m^{6}A methylation patterns between three organs in *Arabidopsis thaliana*. Genome Biol 2015;16:272.
[65] Riviere G, Klopp C, Ibouniyamine N, Huvet A, Boudry P, Favrel P. GigaTON: an extensive publicly searchable database providing a new reference transcriptome in the Pacific oyster *Crassostrea gigas*. BMC Bioinformatics 2015;16:401.
[66] McLean KW, Whiteley AH. RNA synthesis during the early development of the Pacific oyster *Crassostrea gigas*. Exp Cell Res 1974;87:132–8.
[67] Shima H, Matsumoto M, Ishigami Y, Ebina M, Muto A, Sato Y, et al. *S*-adenosylmethionine synthesis is regulated by selective N^6-adenosine methylation and mRNA degradation involving METTL16 and YTHDC1. Cell Rep 2017;21:3354–63.
[68] Huang H, Weng H, Zhou K, Wu T, Zhao BS, Sun M, et al. Histone H3 trimethylation at lysine 36 guides m^{6}A RNA modification co-transcriptionally. Nature 2019;567:414–9.
[69] Wang Y, Li Y, Yue M, Wang J, Kumar S, Wechsler-Reya RJ, et al. N^6-methyladenosine RNA modification regulates embryonic neural stem cell self-renewal through histone modifications. Nat Neurosci 2018;21:195–206.
[70] Lee Y, Choe J, Park OH, Kim YK. Molecular mechanisms driving mRNA degradation by m^{6}A modification. Trends Genet 2020;36:177–88.
[71] Sai L, Li Y, Zhang YY, Zhang J, Qu B, Guo Q, et al. Distinct m^{6}A methylome profiles in poly(A) RNA from *Xenopus laevis* testis and that treated with atrazine. Chemosphere 2020;245:125631.
[72] Kasowitz SD, Ma J, Anderson SJ, Leu NA, Xu Y, Gregory BD, et al. Nuclear m^{6}A reader YTHDC1 regulates alternative polyadenylation and splicing during mouse oocyte development. PLoS Genet 2018;14:e1007412.
[73] Xu C, Wang X, Liu K, Roundtree IA, Tempel W, Li Y, et al. Structural basis for selective binding of m^{6}A RNA by the YTHDC1 YTH domain. Nat Chem Biol 2014;10:927–9.
[74] Lin X, Chai G, Wu Y, Li J, Chen F, Liu J, et al. RNA m^{6}A methylation regulates the epithelial mesenchymal transition of cancer cells and translation of Snail. Nat Commun 2019;10:2065.
[75] Chen J, Sun Y, Xu X, Wang D, He J, Zhou H, et al. YTH domain family 2 orchestrates epithelial-mesenchymal transition/proliferation dichotomy in pancreatic cancer cells. Cell Cycle 2017;16:2259–71.
[76] Li D, Cai L, Meng R, Feng Z, Xu Q. METTL3 modulates osteoclast differentiation and function by controlling RNA stability and nuclear export. Int J Mol Sci 2020;21:1660.
[77] Zhang Y, Gu X, Li D, Cai L, Xu Q. METTL3 regulates osteoblast differentiation and inflammatory response via smad signaling and mapk signaling. Int J Mol Sci 2020;21:199.
[78] Herpin A, Lelong C, Becker T, Rosa F, Favrel P, Cunningham C. Structural and functional evidence for a singular repertoire of BMP receptor signal transducing proteins in the lophotrochozoan

Crassostrea gigas suggests a shared ancestral BMP/activin pathway. FEBS J 2005;272:3424–40.
[79] Le Quéré H, Herpin A, Huvet A, Lelong C, Favrel P. Structural and functional characterizations of an Activin type II receptor orthologue from the pacific oyster *Crassostrea gigas*. Gene 2009;436:101–7.
[80] Bertero A, Brown S, Madrigal P, Osnato A, Ortmann D, Yiangou L, et al. The SMAD2/3 interactome reveals that TGFβ controls m^6A mRNA methylation in pluripotency. Nature 2018;555:256–9.
[81] Brown JA, Kinzig CG, DeGregorio SJ, Steitz JA. Methyltransferase-like protein 16 binds the 3′-terminal triple helix of MALAT1 long noncoding RNA. Proc Natl Acad Sci U S A 2016;113:14013–8.
[82] Shibata N, Kashima M, Ishiko T, Nishimura O, Rouhana L, Misaki K, et al. Inheritance of a nuclear PIWI from pluripotent stem cells by somatic descendants ensures differentiation by silencing transposons in planarian. Dev Cell 2016;37:226–37.
[83] Jankovics F, Bence M, Sinka R, Faragó A, Bodai L, Pettkó-Szandtner A, et al. *Drosophila small ovary* gene is required for transposon silencing and heterochromatin organization, and ensures germline stem cell maintenance and differentiation. Development 2018;145:dev170639.
[84] Gerdes P, Richardson SR, Mager DL, Faulkner GJ. Transposable elements in the mammalian embryo: pioneers surviving through stealth and service. Genome Biol 2016;17:100.
[85] Petton B, Boudry P, Alunno-Bruscia M, Pernet F. Factors influencing disease-induced mortality of Pacific oysters *Crassostrea gigas*. Aquac Environ Interact 2015;6:205–22.
[86] Riviere G, Fellous A, Franco A, Bernay B, Favrel P. A crucial role in fertility for the oyster angiotensin-converting enzyme orthologue CgACE. PLoS One 2011;6:e27833.
[87] Zeng Y, Wang S, Gao S, Soares F, Ahmed M, Guo H, et al. Refined RIP-seq protocol for epitranscriptome analysis with low input materials. PLoS Biol 2018;16:e2006092.
[88] Dobin A, Davis CA, Schlesinger F, Drenkow J, Zaleski C, Jha S, et al. STAR: ultrafast universal RNA-seq aligner. Bioinformatics 2013;29:15–21.
[89] Li B, Ruotti V, Stewart RM, Thomson JA, Dewey CN. RNA-seq gene expression estimation with read mapping uncertainty. Bioinformatics 2010;26:493–500.
[90] Cui X, Meng J, Zhang S, Chen Y, Huang Y. A novel algorithm for calling mRNA m^6A peaks by modeling biological variances in MeRIP-seq data. Bioinformatics 2016;32:i378–85.
[91] Cui X, Wei Z, Zhang L, Liu H, Sun L, Zhang SW, et al. Guitar: an R/Bioconductor package for gene annotation guided transcriptomic analysis of RNA-related genomic features. Biomed Res Int 2016;2016:8367534.
[92] Camacho C, Coulouris G, Avagyan V, Ma N, Papadopoulos J, Bealer K, et al. BLAST+: architecture and applications. BMC Bioinformatics 2009;10:421.
[93] Cock PJA, Chilton JM, Grüning B, Johnson JE, Soranzo N. NCBI BLAST+ integrated into Galaxy. Gigascience 2015;4:39.
[94] Altschul SF, Madden TL, Schäffer AA, Zhang J, Zhang Z, Miller W, et al. Gapped BLAST and PSI-BLAST: a new generation of protein database search programs. Nucleic Acids Res 1997;25:3389–402.
[95] Bindea G, Mlecnik B, Hackl H, Charoentong P, Tosolini M, Kirilovsky A, et al. ClueGO: a Cytoscape plug-in to decipher functionally grouped Gene Ontology and pathway annotation networks. Bioinformatics 2009;25:1091–3.
[96] Larsson J. eulerr: area-proportional Euler and Venn diagrams with ellipses. A bachelor thesis. Lund University; 2018.
[97] Gu Z, Eils R, Schlesner M. Complex heatmaps reveal patterns and correlations in multidimensional genomic data. Bioinformatics 2016;32:2847–9.
[98] Gómez-Rubio V. ggplot2 - elegant graphics for data analysis. J Stat Softw 2017;77:1–3.
[99] Chen T, Chen X, Zhang S, Zhu J, Tang B, Wang A, et al. The Genome Sequence Archive Family: toward explosive data growth and diverse data types. Genomics Proteomics Bioinformatics 2021;19:578–83.